Available online at www.sciencedirect.com

ScienceDirect

Nuclear and Particle Physics Proceedings 273–275 (2016) 425–432

www.elsevier.com/locate/nppp

Sommerfeld enhancements and relic abundance of neutralino dark matter in the general MSSM ☆

Pedro Ruiz-Femenía*

Instituto de Física Corpuscular (IFIC), CSIC-Universitat de València, Apdo. Correos 22085, E-46071 Valencia, Spain

Abstract

We discuss the calculation of Sommerfeld enhancements on the neutralino LSP relic abundance calculation for heavy neutralino dark matter including co-annihilations of nearly mass-degenerate neutralino and chargino states. A newly developed EFT framework enables us to consider for the first time all (off)-diagonal potential and annihilation matrices including P- and next-to-next-to-leading order S-wave effects for a generic MSSM parameter space point, and to treat effects from heavy states perturbatively.

Keywords: Cosmology of Theories beyond the SM, Supersymmetric Standard Model, Nonperturbative Effects

1. Introduction

The search for Dark Matter (DM) is one of the major efforts in particle physics today. Its existence is mainly inferred from its gravitational effects on visible matter, but its composition is still unknown. If dark matter has a particle nature, its characterization will be decisive towards unveiling the broader picture of physics beyond the Standard Model. Amongst the many DM candidates proposed, Weakly Interacting Massive Particles (WIMPs) provide a simple and compelling explanation for this complex physical phenomenon. WIMPs are massive particles produced in the hot early Universe that couple to ordinary matter via a weak-scale interaction, and with a lifetime longer than the age of the Universe in order to have survived until today. WIMPs have the virtue of naturally achieving the correct DM relic density and arise naturally in theories that extend the Standard Model of particle physics. The best motivated candidates are those that arise in models constructed to solve the electroweak symmetry breaking problem, and certainly the most studied is the neutralino lightest supersymmetric particle (LSP) in the minimal supersymmetric standard model (MSSM). The increasing precision in the measurement of the DM relic abundance and of the indirect searches that look for the annihilation products of DM particles, can be thus used to place strong bounds on the MSSM parameter space, complementary to those from colliders and direct detection. For heavy neutralino LSP, given that the LHC and current direct detection experiments does not constrain the neutralino and charging sector much, the astrophysics observations indeed provide the most stringent limits.

Both the current DM density and hence the signals in indirect-detection observations are controlled by the rate at which DM particles annihilate into Standard Model final states. The annihilation cross sections for the nonrelativistic DM have been typically computed with perturbative methods at the leading order in most of the work in the literature, which was justified given the limited accuracy of the observational data collected for the relic density and cosmic rays signatures in the past years. With the increasing precision on these measurements, specially for the DM relic

☆Work done in collaboration with M. Beneke and C. Hellmann.

*Supported by the Spanish Government and ERDF funds from the EU Commission [Grants No. FPA2011-23778, No. CSD2007-00042 (Consolider Project CPAN)] and by Generalitat Valenciana under Grant No. PROMETEOII/2013/007.

Email address: ruiz@ific.uv.es (Pedro Ruiz-Femenía)

http://dx.doi.org/10.1016/j.nuclphysbps.2015.09.062

density, whose value is extracted nowadays with few percent level accuracy [1], several studies have been performed to refine the theoretical calculations at a level comparable with the experimental uncertainties. In the context of supersymmetric DM, the one-loop radiative corrections to the annihilation cross section have been computed in some scenarios: for neutralino co-annihilations with nearly mass-degenerate charginos and sfermions, the complete next-to-leading order QCD contributions [2, 3, 4, 5, 6], as well as an important part of the electroweak ones [7, 8, 9], are already known.

For heavy neutralino DM there is a well-known class of radiative corrections that can become larger than naively expected by the weak nature of the interaction. The so-called Sommerfeld effect, first pointed out in the annihilation (wino- or higgsino-like) neutralino DM into two photons [10], arises when the mutual interaction between the non-relativistic DM particles significantly distorts their wave function, such that they have a larger probability to undergo annihilation. In terms of Feynman diagrams the effect arises from the exchange of the electroweak gauge bosons between the DM particles, which contributes a factor $M_{\rm DM}g^2/M_W$, such that each additional exchanged particle is not suppressed by g^2 when the DM mass is much larger than the mediator mass, eventually requiring a resummation of diagrams to all orders in g^2 in order to correctly calculate the annihilation cross section.

Sommerfeld corrections to the relic density and to indirect signals cosmic have been studied extensively in the pure-wino and Higgsino limits [11, 12, 13, 14, 15, 16], providing important constraints to the neutralino masses. To be able to answer the question of which region of the MSSM parameter space around the wino and higgsino limits is excluded by the available data, the analysis must allow for the neutralino LSP to be in an arbitrary admixture of the electroweak gauginos and higgsinos (work in this direction was initiated in [17, 18]).

In Refs. [19, 20, 21] we have developed an effective field theory formalism that allows to calculate the enhanced radiative corrections to the pair-annihilation of non-relativisitic neutralinos and charginos in the general MSSM with neutralino LSP with arbitrary composition. Our method builds upon the non-relativistic nature of the pair of annihilating particles and separates the short-distance annihilation process (taking place at distances $\sim 1/m_{\rm LSP}$) from the long-distance interactions characterized by the Bohr radius $\sim 1/m_{\rm LSP}g^2$, responsible for the Sommerfeld effect, in analogy to the NRQCD treatment of quarkonium annihilation [22]. However, in the MSSM co-annihilation effects of the LSP with heavier neutralino and chargino species have to be accounted for in regions where mass degeneracies are generic. Dealing with many nearly mass-degenerate scattering states (channels) requires an extension of the conventional NRQCD setup, which is briefly described next. For details we refer the reader to [19, 20, 21].

2. Effective theory approach

The non-relativistic MSSM (NRMSSM) is designed to describe the dynamics of charginos and neutralinos which are off-shell by an amount of the order of $(m_{\rm LSP}v)^2$, where $m_{\rm LSP}$ is the mass of the lightest neutralino and v a typical non-relativistic velocity. The framework allows one to compute the inclusive annihilation rates of pairs of charginos and neutralinos moving at small velocities including their mutual interaction in a systematic expansion in the coupling constant and the velocity. The NRMSSM can account for several non-relativistic particle species, namely those neutralinos and charginos whose masses are nearly degenerate with $m_{\rm LSP}$, and includes potential interactions generated by massive gauge bosons (*i.e.* Yukawa-like potentials) and Coulomb-like potentials. The structure of the EFT Lagrangian reads [19]:

$$\mathcal{L}^{\rm NRMSSM} = \mathcal{L}_{\rm kin} + \mathcal{L}_{\rm pot} + \delta\mathcal{L}_{\rm ann} + \dots \qquad (1)$$

$\mathcal{L}_{\rm kin}$ contains the bilinear terms in the two-component spinor fields ξ_i and $\psi_j = \eta_j, \zeta_j$ that represent the non-relativistic neutralinos (χ_i^0) and charginos (χ_j^- and χ_j^+), respectively. For $n_0 \leq 4$ non-relativistic neutralino species and $n_+ \leq 2$ non-relativistic chargino species, $\mathcal{L}_{\rm kin}$ is given by

$$\mathcal{L}_{\rm kin} = \sum_{i=1}^{n_0} \xi_i^\dagger \left(i\partial_t - (m_i - m_{\rm LSP}) + \frac{\vec{\partial}^2}{2m_{\rm LSP}} \right) \xi_i + \sum_{\psi=\eta,\zeta} \sum_{j=1}^{n_+} \psi_j^\dagger \left(i\partial_t - (m_j - m_{\rm LSP}) + \frac{\vec{\partial}^2}{2m_{\rm LSP}} \right) \psi_j \qquad (2)$$

In order to have a consistent power-counting in the amplitudes describing transitions between two-particle states formed from the neutralino and chargino species included in the EFT we need that the mass differences $(m_i - m_{\rm LSP})$ are formally considered of order $m_{\rm LSP}v^2$ [19]. This implies that heavier neutralinos and charginos (as well as further heavy SUSY particles and higher mass Higgs) are not among the degrees of freedom of the effective theory, and their virtual effects can only appear as short-distance corrections to the operators in $\mathcal{L}^{\rm NRMSSM}$. In the same way, the hard modes associated to the SM and light Higgs-particle produced in

neutralino and chargino pair-annihilations are encoded in the Wilson coefficients of four-fermion operators in $\delta\mathcal{L}_{\rm ann}$, which are local in space-time because the annihilation takes place at short-distances $\sim O(1/m_{\rm LSP})$, as compared to the characteristic range $\sim O(1/m_{\rm LSP}v)$ of the non-relativistic interactions between the chargino and neutralino pairs.

The term $\mathcal{L}_{\rm pot}$ accounts for the exchange of SM gauge bosons and Higgs particles between the two-particle states $\chi_{e_1}\chi_{e_2}$ and $\chi_{e_4}\chi_{e_3}$ ($\chi_{e_i} = \chi^0_{e_i}, \chi^\pm_{e_i}$). For small relative velocity $v_{\rm rel}$ in the two-particle system, such interactions become instantaneous but spatially non-local, and are described in the EFT by 4-fermion operators whose matching coefficients are Yukawa- and Coulomb potentials depending on the relative distance r in the two-body system. In our work we account for $O(v^2_{\rm rel})$ effects in the (co-)annihilation of neutralino and chargino pairs coming from the short-distance part of the annihilation but ignore $O(v^2_{\rm rel})$ contributions from the long-range part. Consequently, only the leading-order Coulomb- and Yukawa potential interactions need to be considered in $\mathcal{L}_{\rm pot}$. A leading-order potential contribution in the basis of total spin ($S = 0, 1$) and in coordinate space has the form

$$V_{\{e_1e_2\}\{e_4e_3\}}(r) = (a_{e_1e_2e_4e_3} - (3-4S)\, b_{e_1e_2e_4e_3})\,\frac{e^{-m_X r}}{r}$$

for the case of the exchange of a boson with mass m_X, among the $\chi\chi$ pairs. Compact analytic expressions for all the potential interactions among the chargino and neutralino pairs in the general MSSM have been derived in [21]. For leading-order scalar boson and photon exchange, the coefficient $b_{e_1e_2e_4e_3}$ vanishes. For Z- and W-boson exchange the spin-dependent part of the potential arises from the axial-vector coupling.

The short-distance annihilation of the chargino and neutralino pairs into SM and light Higgs final states is reproduced in the EFT by local four-fermion operators contained in $\delta\mathcal{L}_{\rm ann}$. The Wilson coefficients of these operators can be determined by matching the MSSM amplitudes for the process $\chi_{e1}\chi_{e_2} \to \chi_{e_4}\chi_{e_3}$ with SM and light Higgs intermediate states with the tree-level matrix element of the EFT operators. For the computation of the neutralino and chargino inclusive annihilation rates the matching can be done for the absorptive part of the amplitude only. At lowest order in the $SU(2)_L$ gauge coupling g_2, the contributions to the Wilson coefficients arise from the absorptive part of $\chi_{e1}\chi_{e_2} \to X_AX_B \to \chi_{e_4}\chi_{e_3}$ 1-loop diagrams with two SM or light Higgs particles in the intermediate state, X_AX_B, and are of $O(\alpha_2^2)$, where $\alpha_2 = g_2^2/4\pi$. The leading-order terms in $\delta\mathcal{L}_{\rm ann}$ are given by dimension-6 four-fermion operators, that describe leading-order S-wave neutralino and chargino annihilation processes $\chi_{e1}\chi_{e_2} \to \chi_{e_4}\chi_{e_3}$. They read [19]

$$\delta\mathcal{L}^{d=6}_{\rm ann} = \sum_{e_i}\ \frac{1}{4}\, f^{\chi\chi\to\chi\chi}_{\{e_1e_2\}\{e_4e_3\}}\left({}^{2S+1}S_S\right)\, O^{\chi\chi\to\chi\chi}_{\{e_4e_3\}\{e_2e_1\}}\left({}^{2S+1}S_S\right) \tag{3}$$

where $f^{\chi\chi\to\chi\chi}_{\{e_1e_2\}\{e_4e_3\}}\left({}^{2S+1}S_J\right)$ are the corresponding Wilson coefficients, which will be often abbreviated as $f\left({}^{2S+1}S_J\right)$. The explicit form of the dimension-6 S-wave operators with $S = 0, 1$ is

$$O^{\chi\chi\to\chi\chi}_{\{e_4e_3\}\{e_2e_1\}}\left({}^1S_0\right) = \chi^\dagger_{e_4}\chi^c_{e_3}\,\chi^{c\dagger}_{e_2}\chi_{e_1} \tag{4}$$

$$O^{\chi\chi\to\chi\chi}_{\{e_4e_3\}\{e_2e_1\}}\left({}^3S_1\right) = \chi^\dagger_{e_4}\sigma^i\chi^c_{e_3}\,\chi^{c\dagger}_{e_2}\sigma^i\chi_{e_1} \tag{5}$$

The sum in (3) is taken over all neutralino and chargino scatering reactions $\chi_{e_1}\chi_{e_2} \to \chi_{e_4}\chi_{e_3}$, and spin $S = 0, 1$. At $O(v^2_{\rm rel})$ in the non-relativistic expansion in momenta and mass differences, dimension-8 four-fermion operators contribute to $\delta\mathcal{L}_{\rm ann}$, which reproduce P-wave and $v^2_{\rm rel}$-suppressed S-wave annihilations. The absorptive parts of the Wilson coefficients, $\hat{f}\left({}^{2S+1}L_J\right)$, have been calculated for the dimension-6 and dimension-8 operators in the MSSM at $O(\alpha_2^2)$ in [19] and [20], respectively. A master formula and necessary ingredients to obtain the contributions to $\hat{f}\left({}^{2S+1}L_J\right)$ from individual states X_AX_B in analytic form can be found therein.

2.1. Sommerfeld-corrected cross section

The spin-averaged center-of-mass frame $\chi_i\chi_j$ annihilation cross section summed over all accessible light final states is given by the imaginary part of the forward-scattering amplitude $\chi_i\chi_j \to \chi_i\chi_j$ by virtue of unitarity, see Fig. 1. In the non-relativistic effective theory, including up to $O(v^2_{\rm rel})$ corrections, this observable is obtained as

$$\sigma^{\chi_i\chi_j\to\,\rm light}\, v_{\rm rel} \;=\; \left(\frac{1}{4}\sum_{s_i,s_j}\right) 2\,{\rm Im}\,\langle\chi_i\chi_j|\,\delta\mathcal{L}_{\rm ann}\,|\chi_i\chi_j\rangle \tag{6}$$

with $v_{\rm rel} = |\vec{v}_i - \vec{v}_j|$ the relative velocity of the annihilating particles in the cms frame. The matrix-elements of four-fermion operators in (6) account for the long-distance interactions between the annihilating pair, while the short-distance annihilation into light particles is described by the Wilson coefficients.

It is well-known from quarkonium physics that matrix-elements of four-fermion operators analogous to those in (6) can be expressed in terms of non-relativistic wave functions and their derivatives evaluated at the origin. For instance, the matrix element of the operator

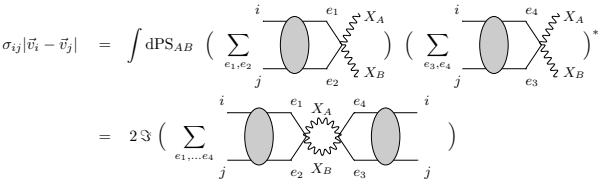

Figure 1: Diagrammatic relation among the annihilation amplitude and the absorptive part of the corresponding forward scattering amplitude in the presence of long-range potential interactions.

$O^{\chi_{e_1}\chi_{e_2}\to\chi_{e_4}\chi_{e_3}}({}^1S_0)$ can be written as

$$\begin{aligned}&\langle\chi_i\chi_j|\chi^\dagger_{e_4}\chi^c_{e_3}|0\rangle\,\langle 0|\chi^{c\dagger}_{e_2}\chi_{e_1}\,|\chi_i\chi_j\rangle\\&=\Big[\,\langle\xi^{c\dagger}_j\xi_i\rangle\,(\psi^{(0,0)}_{e_4e_3,ij}+\psi^{(0,0)}_{e_3e_4,ij})\Big]^*\,\langle\xi^{c\dagger}_j\xi_i\rangle\,(\psi^{(0,0)}_{e_1e_2,ij}+\psi^{(0,0)}_{e_2e_1,ij})\end{aligned}$$

where $\psi^{(L,S)}_{e_1e_2,ij}$ is the $\chi_{e_1}\chi_{e_2}$-component of the scattering wave function for an incoming $\chi_i\chi_j$ state with orbital quantum number L and total spin S, evaluated for zero relative distance and normalized to the free scattering solution. The symbols ξ_i, ξ_j denote the Pauli spinor of the incoming particles χ_i and χ_j. The multi-component wave function $\vec{\psi}^{(L,S)}_{ij}$ accounts for the potential interactions of the incoming $\chi_i\chi_j$ state with all possible intermediate two-body chargino and neutralino states with the same charge and identical spin and partial-wave configuration. Both wave-function components e_1e_2 and e_2e_1 are generated by the matrix-element of operator $\chi^{c\dagger}_{e_2}\chi_{e_1}$; for an operator with quantum numbers L and S, there is a relative sign $(-1)^{L+S}$ between the two components. The lowest-order perturbative result for the matrix-elements of four-fermion operators is obtained by replacing $\psi^{(L,S)}_{e_ae_b,ij}\to\delta_{e_ai}\,\delta_{e_bj}$.

We define for an incoming state $\chi_i\chi_j$ with cms energy $\sqrt{s}$ the Sommerfeld enhancement factor associated to a generic Wilson coefficient, $\hat{f}$, describing the short-distance annihilation of $\chi\chi$ states with spin S and orbital-momentum L as the ratio

$$S_{ij}[\hat{f}({}^{2S+1}L_J)]=\frac{\Big[\psi^{(L,S)}_{e_4e_3,ij}\Big]^*\,\hat{f}^{\chi\chi\to\chi\chi}_{\{e_1e_2\}\{e_4e_3\}}({}^{2S+1}L_J)\,\psi^{(L,S)}_{e_1e_2,ij}}{\hat{f}^{\chi\chi\to\chi\chi}_{\{ij\}\{ij\}}({}^{2S+1}L_J)|_{\rm LO}}\tag{7}$$

A sum over all two-particle states $\chi_{e_1}\chi_{e_2}$ and $\chi_{e_4}\chi_{e_3}$ that have the same charge as the incoming $\chi_i\chi_j$ pair is understood in (7). The Sommerfeld factors are functions of $\sqrt{s}$ or, equivalently, of the relative velocity $v_{\rm rel}$ in the incoming state, which parametrize the long-distance corrections to the annihilation rate of the state $\chi_i\chi_j$. In terms of the Sommerfeld factors, the spin-averaged annihilation cross section (6) acquires a simple form:

$$\begin{aligned}&\sigma^{\chi_i\chi_j\to\,\rm light}\,v_{\rm rel}\\&=S_{ij}[\hat{f}_h({}^1S_0)]\;\hat{f}_{\{ij\}\{ij\}}({}^1S_0)+\;S_{ij}[\hat{f}_h({}^3S_1)]\;3\,\hat{f}_{\{ij\}\{ij\}}({}^3S_1)\\&+\frac{\vec{p}^{\,2}_{ij}}{M^2_{ij}}\Big(S_{ij}[\hat{g}_\kappa({}^1S_0)]\;\hat{g}_{\{ij\}\{ij\}}({}^1S_0)+S_{ij}[\hat{g}_\kappa({}^3S_1)]\;3\,\hat{g}_{\{ij\}\{ij\}}({}^3S_1)\\&+S_{ij}\Big[\frac{\hat{f}({}^1P_1)}{M^2}\Big]\;\hat{f}_{\{ij\}\{ij\}}({}^1P_1)+S_{ij}\Big[\frac{\hat{f}({}^3P_{\mathcal{J}})}{M^2}\Big]\;\hat{f}_{\{ij\}\{ij\}}({}^3P_{\mathcal{J}})\Big)\,,\end{aligned}\tag{8}$$

where $\vec{p}_{ij}=2\mu_{ij}(\sqrt{s}-M_{ij})+O(\vec{p}^{\,4}_{ij})$ is the relative momentum of particles χ_i, χ_j in their cms frame, and M_{ij}, μ_{ij} are the total and reduced mass, respectively, of the two-particle system. The exact meaning of the various Wilson coefficients appearing in (8) is explained in [21]. The pure tree-level annihilation rate with no long-distance corrections is readily recovered by setting all the Sommerfeld factors in (8) to one. The tree-level annihilation cross section thus obtained depends only on the diagonal entry of the Wilson coefficients corresponding to channel $\chi_i\chi_j$.

The non-relativistic matrix elements that define $\psi^{(L,S)}_{e_1e_2,ij}$ receive large quantum corrections, which have to be summed to all orders. Diagramatically, the enhancement originates from the potential loop momentum region of ladder diagrams, whose resummation can be related to the solution of a multi-channel Schrödinger equation. For angular momentum $L=0$ and $L=1$ one can prove that

$$\psi^{(0,S)}_{e_1e_2,ij}=[\psi_E(0)]_{e_1e_2,ij}\;,\;\;\vec{p}\,\psi^{(1,S)}_{e_1e_2,ij}=-i\,[\vec{\nabla}\psi_E(0)]_{e_1e_2,ij}$$

where $[\psi_E(\vec{r})]_{a,ij}$ is the coordinate-space scattering wave-function, which carries two compound indices referring to two-particle states. The second, $i=ij$, refers to the incoming two-particle state with energy $\sqrt{s}=2m_{\rm LSP}+E$ in the cms frame of the annihilation. The first, $e=e_1e_2$, specifies that only the component of the wave-function proportional to the two-particle state e for this incoming state is picked out by the annihilation operator $\chi^{c\dagger}_{e_2}\chi_{e_1}$ that defines $\psi^{(L,S)}_{e_1e_2,ij}$. The scattering solutions $[\psi_E(\vec{r})]_{a,ij}$ can be obtained directly from the matrix-Schrödinger equation

$$\left(\left[-\frac{\vec{\nabla}^{\,2}}{2\mu_a}-E+M_a-2m_{\rm LSP}\right]\delta^{ab}+V^{ab}(r)\right)[\psi_E(\vec{r})]_{b,i}=0\tag{9}$$

The dependence on the initial scattering state appears only in the initial condition for the solution as indicated by the subscript i of $[\psi_E(\vec{r})]_{bi}$, but not in the equation itself. We can solve the matrix-Schrödinger equation for

the Sommerfeld factors (*i.e.* for the values of $[\psi_E(r)]_{a,i}$ and its derivative at the origin) following closely the method described in [23]. The relevant quantity is the matrix T [23, 21] which can be expressed as the inverse of a matrix built from the large-r behaviour of the regular linear independent solutions $[u_L(r)]_{ai}$ of (9). This is explained in detail in [21].

The procedure works well when *all* N states included in the multi-channel Schrödinger equation are degenerate to a high degree. This is the case in MSSM parameter regions where the Sommerfeld enhancement is most effective, such as the wino or Higgsino limit for the neutralino, and when the other states not related to the wino or Higgsino electroweak multiplet are decoupled and ignored. However, we wish to compute the Sommerfeld-enhanced radiative corrections in a larger part of the MSSM parameter space, when the mass splittings become larger than in the wino or Higgsino limit. In this case the method outlined above encounters severe numerical problems and fails to provide accurate results for the Sommerfeld factors. The numerical instability originates from the presence of kinematically closed two-particle states ($M_b > \sqrt{s}$) in the intermediate stage of the annihilation process. The solution for the closed channel involves an exponentially growing component proportional to $e^{\kappa_b r}$ where $\kappa_b^2 = m_{\rm LSP}(M_b - \sqrt{s})$. Eventually, when mass-splittings become larger than $m_W^2/M_{\rm DM}$, the open-channel solutions inherit the exponential growth from the closed channels due to the off-diagonal potentials that mediate the channel mixing, and the formally linearly independent solutions $[u_L]_{ai}$ for the open channels become degenerate. The matrix inversion to obtain T can no longer be done in practice for r large enough such that the asymptotic regime is reached, which causes numerical instabilities. Since typically $m_{\rm LSP} \gg m_{\rm W}$ for the DM scenarios of interest, this situation is generic unless all two-particle states included in the computation are very degenerate within a few GeV or less.

In [21] we provide an alternative method that solves this problem by reformulating the Schrödinger problem directly for the entries of the matrix T that yield the Sommerfeld factors, instead of solving for the wave functions. The improved method is an adaptation of the modified variable phase method introduced in [24]. Leaving aside limitations related to the CPU time needed to solve a system of many coupled differential equations, this method allows to compute the Sommerfeld factors reliably also when many non-degenerate two-particle channels are present. For details on the implementation of the method and examples of its performance we refer the reader to [21].

As an illustration of the general use and potential of our framework, we discuss next the Sommerfeld enhancements in the relic abundance calculation within a realistic wino-like scenario. The investigation of the effect on the relic abundance in other well-motivated MSSM benchmarks with heavy neutralino LSP is the subject of a forthcoming publication [25].

3. Example: Wino-like χ_1^0

Wino-like χ_1^0 DM arranges into an approximate $SU(2)_L$ fermion triplet together with the two chargino states $\chi_1^\pm$. All states $\chi_1^0, \chi_1^\pm$ share the same O(TeV) mass scale, characterised by the wino mass parameter, $m_\chi \sim |M_2|$. The tree-level mass splitting between the neutral and the charged components of the triplet happens to be very small, $O(m_W^4/m_{\rm SUSY}^3)$, and the one-loop radiative corrections dominate this mass difference.

A realistic pMSSM scenario with wino-like χ_1^0 is provided by the SUSY spectrum with model ID 2392587 in [26]. For the latter scenario, the χ_1^0 constitutes a rather pure wino, $|Z_{N\,21}|^2 = 0.999$, with a mass $m_{\rm LSP} \equiv m_{\chi_1^0} = 1650.664\,\text{GeV}$. The mass of the chargino partner $\chi_1^\pm$ is such that $\delta m = m_{\chi_1^+} - m_{\chi_1^0} = 0.155\,\text{GeV}$. In addition, in the pMSSM model 2392587, the bino-like χ_2^0 is only about 8% heavier than the χ_1^0. Hence the χ_2^0 is a potentially relevant co-annihilating particle as well. Sommerfeld enhancements on the co-annihilation rates are taken into account by including in the multi-state Schrödinger equation all $\chi\chi$ two-particle states with mass smaller than $M_{\rm max} = 2\,m_{\chi_1^0} + m_{\chi_1^0} v_{\rm max}^2$, where we set $v_{\rm max} = 1/3$. This choice is motivated by the fact that $v_{\rm max}$ roughly corresponds to the χ_1^0's mean velocity around freeze-out, hence these states are potentially relevant for co-annihilation processes. The remaining heavier two-particle states with mass above $M_{\rm max}$ are included in the computation of the Sommerfeld enhancement of the lighter states in the last loop before the annihilation, following the method developed in [21]. The $\chi\chi$-channels whose long-distance interactions are treated exactly in a pure-wino DM scenario are $\chi_1^0\chi_1^0$, $\chi_1^+\chi_1^-$ in the neutral sector, and $\chi_1^0\chi_1^\pm$ and $\chi_1^\pm\chi_1^\pm$ in the single-charged and double-charged sectors, respectively. In the pMSSM scenario, and in accordance with the rule above that defines the channels which enter the Schrödinger equation, we have to add in addition those states where χ_1^0 is replaced by χ_2^0, *i.e.* $\chi_1^0\chi_2^0$ and $\chi_2^0\chi_1^\pm$. Since χ_2^0 is a bino-like neutralino, essentially neither couples to the wino-like particles nor to gauge bosons, and because sfermion states are rather heavy, potential interactions as well as tree-level annihilation reactions involving the bino-

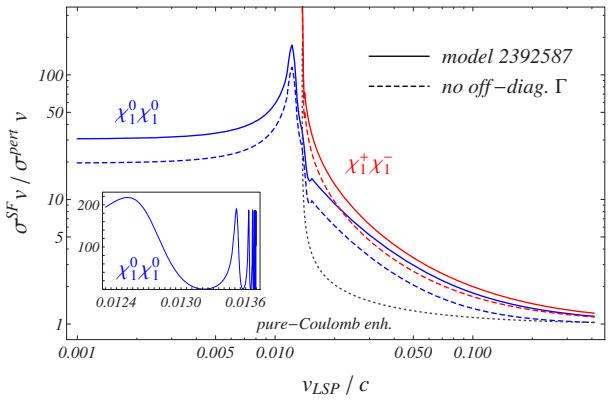

Figure 2: The enhancement $(\sigma^{SF}v)/(\sigma^{pert}v)$ of the $\chi_1^0\chi_1^0$ and $\chi_1^+\chi_1^-$ annihilation cross sections for Snowmass model 2392587.

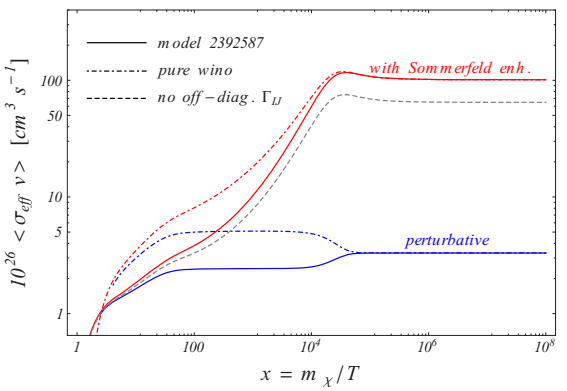

Figure 3: Effective annihilation rate $\langle\sigma_{\rm eff}v\rangle$ as a function of the scaled inverse temperature $x = m_{\chi_1^0}/T$ for Snowmass model 2392587.

like χ_2^0 are strongly suppressed with respect to the corresponding interactions with wino-like particles $\chi_1^0, \chi_1^\pm$. As a consequence, χ_2^0 plays essentially no role for Sommerfeld enhancements, and we can focus the discussion on the channels built from the wino-like χ_1^0 and $\chi_1^\pm$ states only.

In Fig. 2 we plot the enhancement $(\sigma^{SF}v)/(\sigma^{\rm pert}v)$ of annihilation rates including long-range interactions, $\sigma^{SF}v$, with respect to the perturbative tree-level result, $\sigma^{\rm pert}v$, for the two-particle states $\chi_1^0\chi_1^0$ and $\chi_1^+\chi_1^-$ as a function of the velocity $v_{\rm LSP}$ of the incoming χ_1^0's in their cms frame, defined by $\sqrt{s} = 2m_{\chi_1^0} + m_{\chi_1^0}v_{\rm LSP}^2$. The tree-level annihilation rates $\sigma^{\rm pert}v$ are calculated from (8) setting all Sommerfeld factors to one, whereas in case of the Sommerfeld-enhanced rates $\sigma^{\rm SF}v$ each partial wave contribution gets multiplied by an enhancement factor related to the two-particle wave-function of the respective incoming state. As there is a small mass splitting between the χ_1^0 and the $\chi_1^\pm$, the threshold for the on-shell production of the heavier neutral state $\chi_1^+\chi_1^-$ opens at $v_{\rm LSP}/c \simeq 0.014$. Well below this threshold, the enhancement for the $\chi_1^0\chi_1^0$ system is velocity-independent and of $O(10)$. This saturation effect is characteristic for Yukawa-type interactions in the kinematic regime where the relative momentum of the incoming state is well below the mass scale of the mediator. At velocities $v_{\rm LSP}$ just below the $\chi_1^+\chi_1^-$ threshold, resonances in the $\chi_1^0\chi_1^0$ channel can be observed. While the main plot in Fig. 2 displays a curve smoothed over this region, we show in the small sub-figure a close-up of the resonance pattern. At larger velocities, the enhancement in the $\chi_1^0\chi_1^0$ channel approaches one as we depart from the non-relativistic regime. Turning to the enhancement in the $\chi_1^+\chi_1^-$ channel, it shows quite a different behaviour right above its threshold: instead of approaching a constant value, the enhancement factor for $\chi_1^+\chi_1^-$ rises increasingly as the velocities of the $\chi_1^\pm$ get smaller. Such a behaviour is expected in the presence of long-range Coulomb interactions, where the enhancement does not saturate because the mediator is massless. The dotted (black) curve in Fig. 2 displays the enhancement factor in the $\chi_1^+\chi_1^-$ system arising from Coulomb photon exchange only. The true enhancement curve, that involves all potential interactions affecting the $\chi_1^+\chi_1^-$ system asymptotically reaches this Coulomb-like behaviour for velocities directly above the $\chi_1^+\chi_1^-$ threshold. For larger velocities in the $\chi_1^+\chi_1^-$ system the presence of the Yukawa potentials leads to a larger enhancement than in case of Coulomb interactions only.

The dashed curves in Fig. 2 show the enhancements for the $\chi_1^0\chi_1^0$ and $\chi_1^+\chi_1^-$ states when off-diagonal terms in the annihilation matrices are (incorrectly) left out. This can lead to a $\lesssim 30\%$ underestimation of the actual enhancement in the $\chi_1^0\chi_1^0$ channel. The effect is less pronounced for the $\chi_1^+\chi_1^-$ channel, as in this case the cross section also gets significant contributions from ${}^3S_1$ annihilations, which are purely diagonal (the $\chi_1^0\chi_1^0$ pair cannot build a ${}^3S_1$ state), and not just from ${}^1S_0$ ones.

The quantity that enters the Boltzmann equation for the neutralino number density is the thermally averaged effective annihilation rate $\langle\sigma_{\rm eff}v\rangle$ [27, 28]. Fig. 3 shows $\langle\sigma_{\rm eff}v\rangle$ as defined in [21] as a function of the inverse scaled temperature $x = m_{\chi_1^0}/T$. The lower solid (blue) curve represents the perturbative (tree-level) annihilation rates while the upper solid (red) and the dashed (gray) lines refer to Sommerfeld-enhanced cross sections including and neglecting off-diagonal annihilation rates, respectively. Let us first note that for $x \lesssim 10$ the

depicted behaviour of $\langle\sigma_{\rm eff}v\rangle$ is unphysical. The mean velocity of the annihilating particles in the plasma scales as $\sqrt{1/x}$ and hence is no longer non-relativistic for $x \lesssim 10$ while the results of our framework strictly apply only to non-relativistic $\chi\chi$ pair-annihilations, *i.e.* for $x \gtrsim 10$. Around $x \sim 20$ the annihilation rates of χ_1^0 and χ_1^+ can no longer maintain chemical equilibrium and the particles start to decouple from the thermal plasma. Hence only the region above $x \sim 20$ is important for the calculation of the relic abundance. Around $x \gtrsim 10^4$ the number densities of the $\chi_1^\pm$ are so strongly Boltzmann suppressed with respect to the χ_1^0 number density, despite the small mass splitting, that the rates of the charginos basically play no role in the effective rate $\langle\sigma_{\rm eff}v\rangle$. After $\chi_1^\pm$ decoupling, $\langle\sigma_{\rm eff}v\rangle$ including the Sommerfeld enhancements becomes constant, which we can infer from the constant enhancement factor for the $\chi_1^0\chi_1^0$ system for very low velocities shown in Fig. 2. Before $\chi_1^\pm$ decoupling, $\langle\sigma_{\rm eff}v\rangle$ including the Sommerfeld enhancements rises with increasing x due to the contributions from the charginos but also due to the velocity-dependent enhancement on the $\chi_1^0\chi_1^0$ system itself for larger relative velocities. On the contrary, the perturbatively determined $\langle\sigma_{\rm eff}v\rangle$ shows a constant behaviour before and after $\chi_1^\pm$ decoupling with a rise only around the decoupling region; the contributions that dominate the perturbative cross sections in the non-relativistic regime are the velocity-independent leading-order S-wave terms.

Fig. 3 also compares $\langle\sigma_{\rm eff}v\rangle$ as calculated from the wino-like pMSSM scenario and from a pure-wino $SU(2)_L$ triplet minimal DM model with the same χ_1^0 mass. While the rates for $\chi_1^0\chi_1^0$ annihilations agree at permille level, the cross sections involving $\chi_1^\pm$ are generically larger by factors of $O(1)$ in the pure-wino model as compared to the pMSSM wino-like model. This can be mainly traced back to the destructive interference between t-channel sfermion and s-channel Z (and Higgs-boson) exchange amplitudes in $\chi_1^+\chi_1^- \to ff$ annihilations in the pMSSM scenario case, while the t-channel sfermion exchange amplitudes are absent in the pure-wino model. In addition the pure-wino case neglects all final state masses which in particular gives rise to larger annihilation rates into the $t\bar{t}$ and electroweak gauge boson final states as compared to the pMSSM scenario, where the non-vanishing masses of all SM particles are taken into account. This accounts for the deviation between the curves in Fig. 3 before $\chi_1^\pm$ decoupling.

Finally we consider the yield $Y = n/s$, defined as the ratio of the number density n of all co-annihilating particle species divided by the entropy density s in the cosmic co-moving frame. The dependence of the yield on the scaled inverse temperature $x = m_{\chi_1^0}/T$ is governed by a Boltzmann equation and the χ_1^0 relic abundance is obtained from the calculated yield today. In Fig. 4 we show the ratio of the yield Y calculated from Sommerfeld-enhanced cross sections in both the pMSSM and the pure-wino model to the corresponding results using perturbative cross sections, $Y_{\rm pert}$, as a function of x. The denominator $Y_{\rm pert}$ in the ratio $Y/Y_{\rm pert}$ differs for the pMSSM and the pure-wino model, which is a consequence of the different effective rates $\langle\sigma_{\rm eff}v\rangle$, see Fig. 3. Further, in case of the pMSSM scenario we show results corresponding to a calculation of Y including (solid blue line) and neglecting (dashed black line) off-diagonal annihilation rates. Around $x \sim 20$ the yields with Sommerfeld enhancements start to depart from the corresponding perturbative results; the enhanced rates delay the freeze-out of interactions, which leads to a reduction of the yield Y compared to the perturbative result $Y_{\rm pert}$. The most drastic reduction in $Y/Y_{\rm pert}$ occurs between $x \sim 20$ and $x \sim 10^3$. In this region the enhancement factors on the cross sections are of $O(10)$ (and not yet $O(10^2)$ as for very large x), leading to $Y/Y_{\rm pert}$ values that deviate from 1 by a few 10%. For $x \gtrsim 10^5$ the fraction $Y/Y_{\rm pert}$ stays constant, meaning that at these temperatures the particle abundances in both the perturbative and Sommerfeld-enhanced calculation are frozen in. In case of the wino-like model we find that the relic densities calculated from the yield today read $\Omega^{\rm pert}h^2 = 0.112$ and $\Omega^{\rm SF}h^2 = 0.066$. Hence taking into account the Sommerfeld effect leads to a reduction of the calculated relic abundance of around 40%. On the other hand, neglecting the off-diagonal annihilations in the calculation of Sommerfeld-enhanced rates overestimates the relic density by 15% compared to the correct $\Omega^{\rm SF}h^2$. Due to overall larger hard annihilation rates in the pure-wino model, the calculated relic

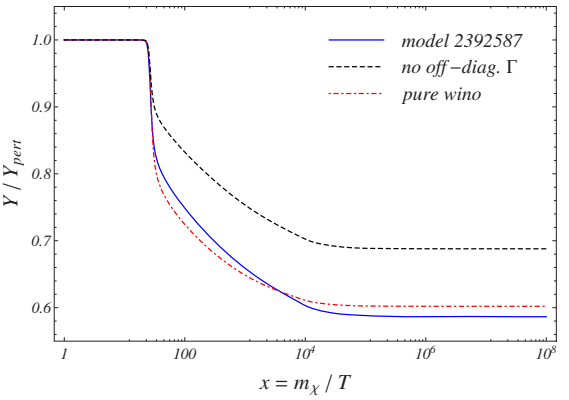

Figure 4: The ratios of the yield $Y/Y_{\rm pert}$ as a function of $x = m_{\chi_1^0}/T$.

density including Sommerfeld-enhanced rates turns out to be $\Omega^{\rm SF}_{\text{pure-w}}h^2 = 0.034$, while the corresponding perturbative result is $\Omega^{\rm pert}_{\text{pure-w}}h^2 = 0.056$.

References

[1] **Planck Collaboration** Collaboration, P. Ade *et al.*, arXiv:1303.5076 [astro-ph.CO].

[2] B. Herrmann and M. Klasen, *Phys.Rev.* **D76** (2007) 117704, arXiv:0709.0043 [hep-ph].

[3] B. Herrmann, M. Klasen, and K. Kovarik, *Phys.Rev.* **D79** (2009) 061701, arXiv:0901.0481 [hep-ph].

[4] B. Herrmann, M. Klasen, and K. Kovarik, *Phys.Rev.* **D80** (2009) 085025, arXiv:0907.0030 [hep-ph].

[5] J. Harz, B. Herrmann, M. Klasen, K. Kovarik, and Q. L. Boulc'h, *Phys.Rev.* **D87** (2013) no. 5, 054031, arXiv:1212.5241.

[6] B. Herrmann, M. Klasen, K. Kovarik, M. Meinecke, and P. Steppeler, *Phys.Rev.* **D89** (2014) 114012, arXiv:1404.2931 [hep-ph].

[7] N. Baro, F. Boudjema, and A. Semenov, *Phys.Lett.* **B660** (2008) 550–560, arXiv:0710.1821 [hep-ph].

[8] N. Baro, F. Boudjema, and A. Semenov, *Phys.Rev.* **D78** (2008) 115003, arXiv:0807.4668 [hep-ph].

[9] N. Baro, F. Boudjema, G. Chalons, and S. Hao, *Phys.Rev.* **D81** (2010) 015005, arXiv:0910.3293 [hep-ph].

[10] J. Hisano, S. Matsumoto, M. M. Nojiri, and O. Saito, *Phys.Rev.* **D71** (2005) 063528, arXiv:hep-ph/0412403 [hep-ph].

[11] J. Hisano, S. Matsumoto, M. Nagai, O. Saito, and M. Senami, *Phys.Lett.* **B646** (2007) 34–38, arXiv:hep-ph/0610249 [hep-ph].

[12] M. Drees, J. Kim, and K. Nagao, *Phys.Rev.* **D81** (2010) 105004, arXiv:0911.3795 [hep-ph].

[13] A. Hryczuk and R. Iengo, *JHEP* **1201** (2012) 163, arXiv:1111.2916 [hep-ph].

[14] J. Fan and M. Reece, *JHEP* **1310** (2013) 124, arXiv:1307.4400 [hep-ph].

[15] T. Cohen, M. Lisanti, A. Pierce, and T. R. Slatyer, *JCAP* **1310** (2013) 061, arXiv:1307.4082.

[16] A. Hryczuk, I. Cholis, R. Iengo, M. Tavakoli, and P. Ullio, *JCAP* **1407** (2014) 031, arXiv:1401.6212 [astro-ph.HE].

[17] A. Hryczuk, R. Iengo, and P. Ullio, *JHEP* **1103** (2011) 069, arXiv:1010.2172 [hep-ph].

[18] A. Hryczuk, *Phys.Lett.* **B699** (2011) 271–275, arXiv:1102.4295 [hep-ph].

[19] M. Beneke, C. Hellmann, and P. Ruiz-Femenia, *JHEP* **1303** (2013) 148, arXiv:1210.7928 [hep-ph].

[20] C. Hellmann and P. Ruiz-Femenia, *JHEP* **1308** (2013) 084, arXiv:1303.0200 [hep-ph].

[21] M. Beneke, C. Hellmann, and P. Ruiz-Femenia, *"Non-relativistic pair annihilation of nearly mass degenerate neutralinos and charginos III. Computation of the Sommerfeld enhancements"*, preprint TUM-HEP-954-14, TTK-14-21, SFB-CPP-14-69, IFIC-14-58.

[22] G. T. Bodwin, E. Braaten, and G. P. Lepage, *Phys.Rev.* **D51** (1995) 1125–1171, arXiv:hep-ph/9407339 [hep-ph].

[23] T. R. Slatyer, *JCAP* **1002** (2010) 028, arXiv:0910.5713 [hep-ph].

[24] S. Ershov, J. Vaagen, and M. Zhukov, *Phys.Rev.* **C84** (2011) 064308.

[25] M. Beneke, C. Hellmann, and P. Ruiz-Femenía, *Heavy neutralino relic abundance with Sommerfeld enhancements – a study of pMSSM benchmarks*, TUM-HEP-955/14, TTK-14-22, SFB/CPP-14-70, IFIC/14-59.

[26] M. W. Cahill-Rowley, J. L. Hewett, A. Ismail, M. E. Peskin, and T. G. Rizzo, arXiv:1305.2419 [hep-ph].

[27] P. Gondolo and G. Gelmini, *Nucl.Phys.* **B360** (1991) 145–179.

[28] J. Edsjo and P. Gondolo, *Phys.Rev.* **D56** (1997) 1879–1894, arXiv:hep-ph/9704361 [hep-ph].